Optimal degradation of organophosphorus pesticide at low levels in water using fenton and photo-fenton processes and identification of by-products by GC-MS/MS

Chemseddine Zekkaoui, Tarek Berrama, David Dumoulin, Gabriel Billon, Yassine Kadmi

Optimal degradation of organophosphorus pesticide at low levels in water using Fenton and photo-Fenton processes and identification of by-products by GC-MS/MS

Chemseddine Zekkaoui[1,2], Tarek Berrama[1], David Dumoulin[2], Gabriel Billon[2], Yassine Kadmi[2,3*]

[1]*Laboratory of Industrial Process Engineering Sciences, University of Sciences and Technology Houari Boumediene, BP 32, El-Alia, 16111, Bab-Ezzouar, Algiers, Algeria*

[2] *Univ. Lille, CNRS, UMR 8516 - LASIRe - Laboratoire Avancé de Spectroscopie pour les Intéractions la Réactivité et l'Environnement, F-59000 Lille, France*

[3]*Université d'Artois, IUT de Béthune, 62400, Béthune, France*

* *Corresponding Author:*

Email: yassine.kadmi@univ-lille.fr

Abstract

This study aiming to determine the optimal conditions to degrade an organophosphate pesticide diazinon (DZN) at low levels concentrations ($\mu g.mL^{-1}$) and to identify the by-products generated. The degradation processes utilized were the Fenton and photo-Fenton. The iron concentration [Fe^{2+}], the hydrogen peroxide concentrations [H_2O_2], and the solution pH are the investigated parameters. The Doehlert three-parameter experimental design was applied to model and optimize both degradation processes. The mathematical models suggested were assessed and validated by application of analysis of variances ANOVA. In the case of Fenton process, the greatest yield of degradation (79%) was obtained at [Fe^{2+}] = 35 $mg.L^{-1}$ (0.63 $mmol.L^{-1}$), [H_2O_2] = 423 $mg.L^{-1}$ (12.44 $mmol.L^{-1}$), and pH = 5.0. In photo-Fenton process, the maximum yield of degradation (96%) was obtained under the conditions of [Fe^{2+}] = 29 $mg.L^{-1}$ (0.52 $mmol.L^{-1}$), [H_2O_2] = 258 $mg.L^{-1}$ (7.59 $mmol.L^{-1}$) and pH = 4.6. QuEChERS (quick, easy, cheap, effective, rugged, and safe), as extraction technique, and GC-MS/MS (gas chromatography coupled with triple quadrupole mass spectrometry) were used to identify the by-products degradation of DZN. The identified compounds are diazoxon, triethyl phosphate, triethyl thiophosphate, 2-isopropyl-5-ethyl-6-methylpyrimidine-4-ol, 2-isopropyl-6-methylpyrimidine-4-ol (IMP) and hydroxydiazinon. Three possible pathways for diazinon degradation have been suggested and the hydroxylation, oxidation and hydrolysis are likely probable degradation mechanisms.

Keywords: degradation; diazinon; water; detection of by-products; advanced oxidation process

1. Introduction

Population growth and human survival require ever-increasing food production, which is largely supported by vital agricultural activities (Sadowski and Baer-Nawrocka, 2018). One group of chemicals used to improve agricultural yield (Malakootian et al., 2020) are pesticides, employed to control pests and weeds and to enhance food production (de Souza et al., 2020). Some of these compounds are known as persistent organic pollutants and thus remain in water for a long time, accumulate in sediments and travel long distances. They exert toxic effects on the environment, human health, and living organisms, even at low concentrations (Katsikantami et al., 2019; Vasseghian et al., 2021; Vasseghian, et al., 2020).

Globally, pesticides are classified into four main families, depending on their use, chemical composition, and nature of active ingredients (Kaur et al., 2019). Herbicides are a class of pesticide used to control or prevent the growth of weeds (Fernanda Pereira Barbosa, 2019). Insecticides are used against insect eggs, larvae, and adult insects, and fungicides are designed to eliminate or limit the development of parasitic plant fungi. Diazinon (DZN), an insecticide and highly toxic organophosphate pesticide (Čolović et al., 2010), is used to control insects in residential, agricultural and livestock areas (Acero et al., 2008). Its presence in surface waters is widespread due to extensive use (Real et al., 2007). For example, in the USA, 6 million kg of DZN are applied annually (Real et al., 2007). Under favorable environmental conditions, it can accumulate in groundwater due to its limited biodegradability (Molla et al., 2019; Raeisi et al., 2016). Several pesticides are usually detected in waters at the concentration range of 1–1000 $\mu g.L^{-1}$ (Jones et al., 2017). DZN has been detected in surface waters at concentrations of 80 $ng.L^{-1}$ to 25 $\mu g.L^{-1}$ in countries such as the USA, Spain, and Canada (Glinski et al., 2018; Metcalfe et al., 2019; Proia et al., 2013). This compound is toxic to humans, inhibiting the enzyme acetylcholinesterase, which is essential for nervous system function (Shirzad-Siboni et al., 2015; Zhang et al., 2010). Fatal human doses were found to be in the range of 90–444 $mg.kg^{-1}$ (Molla et al., 2019). Aquatic system toxicity is 350 $ng.L^{-1}$ with a 48 h LC_{50} of 4.4 $mg.L^{-1}$ in killifish (Daneshvar et al., 2007; Kazemizad et al., 2016). DZN is categorized as a WHO class II compound, considered moderately hazardous (World Health Organization, 2010).

The toxicity of DZN, its resistance to natural decomposition and its persistence in the environment compel us to find methods that eliminate and/or degrade this molecule (Molla et al., 2019). In recent years, several studies have focused on the degradation of pesticides in

aqueous solution by different processes (Al Momani et al., 2004a; Al Momani et al., 2004b; Al Momani et al., 2009, 2007; Contreras et al., 2003). Gar Alalm et al. (2015) attempted to degrade DZN by two processes and found photocatalysis degraded DZN by 40% and photo-Fenton by approximately 50%. Activated carbon prepared from flamboyant pods modified with Fe^{2+} has also been used as a TiO_2 support, and the photocatalytic degradation using this combination was approximately 80% (Hassan et al., 2017). Similarly, using tungsten-doped zinc oxide nanoparticles as a catalyst, Maleki et al. (2020) observed 89% of DZN degradation. Nasrollahi et al. (2020) used a biological approach involving bacterial endophytes in rice plants to degrade DZN (50% degradation). Membrane techniques have also been investigated to eliminate DZN, and nanofibrous membranes eliminated 84% of DZN (Pordel et al., 2019).

Advanced oxidation processes (AOPs) have proven to be particularly effective technologies for the degradation of organophosphate pesticides (Vasseghian et al., 2020; Wang and Shih, 2015). AOPs are based on the intrinsic ability of hydroxyl radicals (OH·) (Moradi et al., 2020a) generated in the case of the Fenton and Photo Fenton processes, by specific chemical reactions in aqueous solution, to promote rapid and non-selective oxidation of organic molecules, thereby promoting their degradation (Kanakaraju et al., 2018; Moradi et al., 2021; Moradi et al., 2020b; Vasseghian et al., 2020). In the others AOPs, the active species may be O_3 (ozonation), O_2 (persulfate-based oxidation), etc. The photo-Fenton process combines the Fenton reagents hydrogen peroxide (H_2O_2) and ferrous ions (Fe^{2+}) in the presence of UV-visible radiation to produce more OH· radicals *via* four reactions: i) a catalytic reaction of H_2O_2 with Fe^{2+} ions, a Fenton reaction (Eq. 1) (Nichela et al., 2013); ii) a Fenton process initiated by Fe^{3+} (Eq. 2); iii) a photo-reduction of Fe^{3+} to Fe^{2+} ions (Eq. 3); and iv) a peroxide photolysis *via* shorter wavelengths (Eq. 4) (Rahim Pouran et al., 2015). Ferrous ions generated in the reaction represented by Eq. 3 allow producing additional hydroxyl radicals. These radicals have a high oxidation potential (E_0) ranging between 2.72 V (Han et al., 2020) and 2.80 V (Singh et al., 2019) and can break down organic compounds such as pesticides (Moradi et al., 2020). In addition, the photo-Fenton reactions cause faster mineralization of organic compounds than the dark reaction due to the presence of UV irradiation or sunlight (Audino et al., 2017).

$$H_2O_2 + Fe^{2+} \rightarrow Fe^{3+} + OH^- + OH\cdot \qquad \text{Eq. 1}$$

$$H_2O_2 + Fe^{3+} \rightarrow Fe^{2+} + H^+ + HO_2\cdot \qquad \text{Eq. 2}$$

$$Fe(OH)^{2+} + h\nu \rightarrow Fe^{2+} + OH\cdot \qquad \lambda < 580\ \text{nm} \qquad \text{Eq. 3}$$

$$H_2O_2 + h\nu \rightarrow 2\,OH\cdot \qquad \lambda < 310\ \text{nm} \qquad \text{Eq. 4}$$

In recent years, statistical methods have been extensively applied for experimental design in many science fields (Hanrahan and Lu, 2006; Doufene et al., 2018; Smaali et al., 2021). Most of experimental designs commonly use parameter screening (Dragoi and Vasseghian, 2020), response modeling and optimization (Callao, 2014). Central Composite, Box-Behnken, and Doehlert, experimental designs employed in Responses Surfaces Methodology (RSM) (Heydari et al., 2018; Moradi et al., 2018), are relevant in modeling and/or optimization (Ferreira et al., 2007). Doehlert design is one of the most commonly used designs because it provides more advantages than Central Composite and Box-Behnken (Callao, 2014; Ferreira et al., 2007).

To date, no study has evaluated the degradation of DZN at trace levels ($\mu g.L^{-1}$) and identified DZN degradation by-products at ultra-trace levels ($ng.L^{-1}$), likely due to the lack of advanced analytical methods and an efficient and rapid extraction protocol. Our study is novel in combining simple and efficient degradation processes, the application of an experimental design to determine the optimal degradation conditions, and the use of efficient extraction and analysis techniques to monitor DZN degradation and to determine degradation by-products at ultra-trace concentrations ($ng.L^{-1}$) in aqueous matrices. We applied advanced oxidation processes (Fenton and photo-Fenton) and a Doehlert design to optimize and model each process. Hydrogen peroxide (H_2O_2), ferrous ions (Fe^{2+}) concentrations and pH were optimized to eliminate efficiently DZN. In the present work, extremely sensitive and reliable techniques based on a QuEChERS (quick, easy, cheap, effective, rugged, and safe) extraction approach and gas chromatography coupled with triple quadrupole mass spectrometry (GC-MS/MS) were used to identify intermediate products in water. The possible pathways of the degradation of DZN were also proposed. We believe our study will inform future experimental studies of organophosphate pesticide pollutant degradation in wastewater, especially DZN.

2. Materials and methods

2.1. Materials and reagents

Diazinon was purchased from Sigma-Aldrich (99%, purity). Its chemical formula is $C_{12}H_{21}N_2O_3PS$ and the International Union of Pure and Applied Chemistry (IUPAC) name is O,O-diethyl O-2-isopropyl-6-methylpyrimidin-4-yl phosphorothioate (CAS: 333-41-5). The molecular weight, the solubility in water at 20°C and the pK_a of DZN are 304.35 $g.mol^{-1}$, 60 $mg.L^{-1}$ and 2.6, respectively. Hydrogen peroxide (33%, *w/w*) and Fe^{2+} ions were produced

from ferrous sulfate heptahydrate ($FeSO_4$, $7H_2O$) as a source of Fe^{2+}. Sodium hydroxide (NaOH) and hydrochloric acid (HCl) solutions were used to adjust the solution pH in each experiment. All chemicals were of analytical reagents grade and purchased from Sigma-Aldrich, France. The ultrapure water (18.2 MΩ.cm of resistivity) was used in this work.

2.2. Diazinon degradation via Fenton and photo-Fenton experiments

All Fenton process experiments were conducted in a 250 mL capacity Pyrex batch reactor with 100 mL of ultrapure water at room temperature in the dark (25 °C). The concentration of the effluent was 1 µg.mL^{-1}, prepared by dissolving DZN in ultrapure water. For Fenton reagents, the added of the DZN concentration was depended on the conditions of each experiment. The photo-Fenton experiments were carried out in a cubical photo-reactor equipped with a cooler to maintain a constant temperature. A Pyrex crystallizer batch reactor with a capacity of 250 mL was used to ensure consistent and direct exposure of the solution to the lamplight supplied by Philips lamp (11 W, UVA).

2.3. Analytical methods

2.3.1. UHPLC/DAD analysis

Diazinon concentration in aqueous solutions was measured using an ultra-high-performance liquid chromatography coupled with a diode array detector (UHPLC/DAD) (Agilent Technology, Model 1260, France). Chromatographic separation was performed with a C18 column (150 mm × 4.6 mm, 2.7 µm) (Agilent Technology, France). The auto-sampler was maintained at 5 °C. Acetonitrile and ultrapure water were used as mobile phases. Isocratic elution mode was applied for chromatographic separation. The eluent used was a mixed solvent of acetonitrile and ultrapure water (60/40, *v/v*). The mobile phase flow rate was 0.4 mL.min^{-1} and the retention time of DZN was 17.8 min. DZN was quantified at $\lambda_{max} = 210$ nm. The UHPLC/DAD was used to evaluate the amount of DZN in the aqueous solution. The degradation yield Y_i of DZN was calculated using equation 5.

$$Y_i = \frac{(C_0 - C_t)}{C_0} \times 100 \qquad \text{(Eq. 5)}$$

in which C_0 and C_t are the DZN initial concentration and DZN concentration at a given time t in mg.L^{-1}, respectively.

2.3.2. GC-MS/MS analysis

The standard solution and sample extracts were analyzed by gas chromatography coupled with triple quadrupole mass spectrometry (GC-MS/MS) (Agilent Technology, 7890B-7000D, France). GC separation was performed using a Phenomenex capillary column ZB-XLB-HT Inferno^{TM} (30 m × 0.25 mm × 0.25 μm). The injection volume was 3 μL. The column temperature program was as follows: the initial temperature was maintained at 75 °C for 2.57 min, increased to 150 °C at a rate of 50 °C/min, increased to 200 °C at 6 °C/min, then to 280 °C at 16 °C/min, and held there for 15 min. The mass spectrometer (MS/MS) was operated with an electron impact (EI) source for detection. The electron energy was 70 eV, and the transfer line temperature was set at 280 °C. The total duration of the analysis was 32.40 min. The mass-to-charge ratio (m/z) of DZN is 304 uma.

2.3.3. QuEChERS extraction method

Before analysis by GC-MS/MS, a QuEChERS (quick, easy, cheap, effective, rugged, and safe) dispersive solid phase extraction (d-SPE) was performed. The extraction followed is based on the principle of d-SPE extraction with an organic solvent in the presence of salts to ensure the transformation of the molecules in the effluent to the organic phase (Drożdżyński and Kowalska, 2009; Iqbal et al., 2020). This recently developed technique can be employed to recover many targets, including highly polar pesticides and highly acidic molecules. The QuEChERS technique can be carried out in two steps. The first one is an extraction using organic solvents (acetonitrile or hexane) and inorganic salts ($MgSO_4$ and NaCl) to separate the water-organic phase, followed by a purification step, utilized to eliminate all interfering components. The proposed technique, based on several studies (Abdel Ghani and Hanafi, 2016; Iqbal et al., 2020; Zaidon et al., 2019), was modified for the present work. The QuEChERS (Interchim, France) extraction technique consists of combining 10 mL of the sample with 10 mL of acetonitrile in an extraction tube containing a mixture of salts. The tube is passed through the vortex for 1 min to mix the two phases. Subsequent centrifugation (3000 rpm) for 5 min ensures sufficient separation of the two phases. In the purification step, 6 mL of the organic phase from the tube used in the first step was transferred to a second tube (clean up tube), vortexed for 30 s, and centrifuged (3000 rpm) for 5 min to provide the final organic solution.

After extraction, the eluate was collected in a 14 mL, conical graduated glass Pyrex tube (VWR, Fontenay-sous-Bois, France). The extract was evaporated to a final volume of 10 µL using a PuriVap-6 system (Interchim, France), under a high-purity nitrogen stream and transferred to a vial for GC-MS/MS analysis.

2.4. Doehlert design methodology

One of the best experimental designs for second-order models is the Doehlert design proposed by D.H Doehlert in 1970 (Ferreira, 2004). It is often preferred over the Central Composite design and Box-Behnken designs as it is easily expended in experimental and variable space (Ferreira et al., 2007). These experimental designs are types of response surface methodologies (RSM). The number of tests ("n") in the Doehlert design depends on multiple factors ("k") according to the equation $n = k(k + 1)$, and one or more central points can be added. Another advantage of this plan is that the number of levels is not the same for each variable, allowing for a free choice of the variables with a small or large number of levels (Ferreira, 2004). In the case of three variables, the first one was studied at five levels, the second one at seven levels, and the last one at three levels, so the variables' position can be chosen according to their importance (Ferreira, 2004).

For modeling and optimization purposes, the experimental data have been explored through a quadratic polynomial model (Eq. 6).

$$\hat{Y} = b_0 + \sum_{i=1}^{n} b_i x_i + \sum_{i=1}^{n} b_{ii} x_i^2 + \sum_{i=1}^{n-1} \sum_{j=i+1}^{n} b_{ij} x_i x_j \qquad \text{(Eq. 6)}$$

in which $\hat{Y}$ is the predicted response, b_0 is a constant, b_i is a linear constant, b_{ij} are the interaction coefficients, b_{ii} are quadratic coefficients, and x_i, x_j are the coded values of the variables. The Doehlert matrix with coded and actual values of variables for each Fenton and photo-Fenton experiment are shown in Table 1.

Table 1

3. Results and discussion

3.1. Development and validation of the predictive regression models

The yields of DZN degradation estimated from the application of Doehlert design are given in Table 1 for each Fenton and photo-Fenton experiment. Two regression models are

suggested, the responses considered are the degradation yield of DZN by Fenton ($\hat{Y}_F$) and photo-Fenton ($\hat{Y}_{Ph-F}$) processes.

The modeling objective is to determine the best regression relationship linking the dependent variables (responses) and the independent variables (factors). Modeling is an important step in the optimization process. It could not be considered reliable if the final model did not provide a significant level of correlation between input and output data. All factors included in the final model must be statistically significant. The level of significance model factor (b of Eq. 6) is determined by estimation of the student parameter value (t_i), which is compared to the critical student value (t_{crit}), determined from Student statistical table (not given in the main text), depending on the model degree of freedom (df) and the significance level (α). Generally, (α) is taken to be equal to 0.05 (5%), it represents the probability value (p-value). A coefficient of model is considered significant if its $|t_i|$ < p-value (Benredouane et al., 2016).

The estimation of model factors shows that in the case of Fenton process, five factors (including the b_0 (see Eq. 6)) are statistically significant, namely $[Fe^{2+}]$, $[H_2O_2]$, $(pH * [H_2O_2])$ and pH^2, and in the case of photo-Fenton process, six factors (including the b_0) are statistically significant, namely $[Fe^{2+}]$, pH, $[Fe^{2+}]^2$, $[H_2O_2]$ and pH^2. All these factors have a p-value < 0.05. The analysis of variance (ANOVA) is used systematically as the main method to validate regression models in design of experiments methodology approach. To validate the suggested models (including only the significant factors), a Fisher test is carried out. The Fisher-value (F-value) of the model (estimated on basis of the ratio between model and residual mean square) and compared to Fisher-Value critical (F_{crit}) were determined from Fisher-Snedecor table with two degrees of freedom (df_1 and df_2) and (α = 5%). For Fenton process model, F-value (df_1= 5, df_2= 7) = 10.80 and for photo-Fenton process model, F-value (df_1= 4, df_2= 8) = 14.46. The F_{crit} are respectively equal to 3.97 and 3.84, then in both cases, F-value > Fcrit, which means that the suggested models are validated at the fixed level of significance. Based on these considerations, final models retained for both processes are given by equations 7 and 8.

$$\hat{Y}_{Ph-F} = 94.0 + 7.9[Fe^{2+}] + 5.1\,pH - 20.0[Fe^{2+}]^2 - 31.4[H_2O_2] - 12.3pH^2 \quad \text{(Eq. 7)}$$

$$\hat{Y}_F = 69.9 + 6.1[Fe^{+2}] + 4.9[H_2O_2] - 10.8\,pH.[H_2O_2] - 11.4pH^2 \quad \text{(Eq. 8)}$$

The predicted values of the DZN degradation yield are estimated for each process and compared with the experimental values; the corresponding plots are shown in Figure 1(a) and (b). The R^2 and adjusted R^2 values obtained were 0.911 and 0.849 for the photo-Fenton and 0.844 and 0.766 for the Fenton process.

3.2. Determination of optimal conditions of degradation

Modde software was used to determine the optimum points for each degradation process. Results show that equation 7 describes a critical point corresponding to a maximum degradation yield (96%); this is shown in Figure 1(c), plotted using the 3D graph. The factor values in this case were $[Fe^{2+}] = 29$ mg.L^{-1} (0.52 mmol.L^{-1}); $[H_2O_2] = 258$ mg.L^{-1} (7.59 mmol.L^{-1}) and pH = 4.6. So, equation 8 does not present a critical point; in this case, the extreme value theorem (Weierstrass) was applied to resolve this problem (Martínez-Legaz, 2014), this is confirmed by plots in 3D graph (Fig 1 (d) and (e)). The highest value corresponding to the optimal value was obtained at the boundary of the study range. As seen in Table 1, the greatest degradation (79%) was obtained under the conditions of run 3, indicating that the optimal conditions were $[Fe^{2+}] = 35$ mg.L^{-1} (0.63 mmol.L^{-1}); $[H_2O_2] = 423$ mg.L^{-1} (12.44 mmol.L^{-1}) and pH = 5.0. Furthermore, the 3D response surface plot shows the highest yield corresponding to optimal values cited previously. However, on the basis of experimental design results and in the case of Fenton process, pH is not a significant parameter. The optimal conditions do not vary therefore greatly when the pH changes but to take in account the conditions of iron precipitation, the pH has been fixed to 3.4 (the low level value).

Figure 1

These results show that the optimal concentrations of Fe^{2+} and H_2O_2 for the photo-Fenton process were lower than those of the Fenton process, and the yield of the degradation was greater using the photo-Fenton process. These results highlight the significant effect of UV-irradiation. When the reaction medium was exposed to artificial light, degradation yield significantly improved with a lower reagent consumption than in the Fenton process: only 29 mg.L^{-1} (0.52 mmol.L^{-1}) of Fe^{2+} and 258 mg.L^{-1} (7.59 mmol.L^{-1}) of H_2O_2 were used instead of 35 mg.L^{-1} (0.63 mmol.L^{-1}) and 423 mg.L^{-1} (12.44 mmol.L^{-1}) of H_2O_2 to obtain 96% instead of 79% for the photo-Fenton and Fenton process, respectively. These findings can be explained by the fact that the ferric ions resulting from photodegradation (Eq. 1) have been photochemically regenerated into ferrous ions according to equations 9 and 10.

$$H_2O_2 + Fe^{3+} + h\nu \rightarrow Fe^{2+} + H^+ + \cdot OH \quad \text{Eq. 9}$$

$$H_2O_2 + Fe^{3+} + h\nu \rightarrow Fe^{2+} + H^+ + \cdot HO_2 \quad \text{Eq. 10}$$

These ions further react with H_2O_2 to produce radical hydroxyl and ferric ions, and in this manner, the cycle continues, as confirmed by other studies (Ameta et al., 2018; Audino et al., 2017; Marchetti and Bessa Azevedo, 2020).

Notably, the ratio of the reagent concentrations (H_2O_2/Fe^{2+}) under the optimal conditions for both processes are different: 20 for the Fenton process and 15 for the photo-Fenton process. These results indicate that the implementation of the process requires the lowest reagent ratio with a maximum of degradation.

3.3. Validation of optimal conditions

An experiment for each process was conducted under the corresponding optimal conditions by following DZN degradation over time. The results are shown in Figure 2.

Figure 2

Our findings displayed that the degradation of DZN was complete after just 15 min for the photo-Fenton process. In contrast, degradation using the Fenton process reached a yield of 85% after one hour of the experiment. The degradation using the photo-Fenton process was faster and more efficient than in the Fenton process, which implies that the light from the UV radiation accelerated the degradation process and improved the performance to achieve complete DZN degradation. From a technical-economic point of view, it should be noted that the use of a lamp in the photo-Fenton process results in slightly higher energy consumption than in the Fenton process.

3.4. Determination of by-products using QuEChERS and GC-MS/MS methods

GC-MS/MS was employed to identify the generated degradation by-products of DZN. In this purpose, three samples were taken to determine the by-products: the 1st one before the process launch (starting point), the 2nd one after 5 min, and the last one at 60 min. A dispersive solid phase extraction using acetonitrile in the QuEChERS protocol (section 2.3.3) was used to analyze these samples. The results of the analysis of each sample are presented with the chromatograms obtained from the GC-MS/MS (Figure 3).

Figure 3

As observed in the chromatograms, the DZN retention time was 17 min, and the molecular weight usually obtained was 304 uma (Fig. 3.a). Several by-products were detected (Fig. 3.b), grouped in Table 2 by their retention time. By comparing Figs. 3.a and 3.b, we notice the disappearance of the DZN peak, implying the total degradation of DZN after 5 min. We can also notice in Figure 3.c that no by-products were detected after 60 min of degradation confirming the total mineralization of DZN (Figure 3.c). These results confirm the results obtained previously. In addition, the by-products found in this work correspond to the results found in previously published studies. In their study of photocatalytic DZN degradation under sunlight irradiation, Molla et al. (2019) revealed eight by-products: diazoxon, triethyl phosphate, triethyl thiophosphate, 2-isopropyl-5-ethyl-6-methylpyrimidine-4-ol, 2-isopropyl-4-ethyl-6-methylpyrimidine-5-ol, 2-isopropyl-6-methylpyrimidine-4-ol and hydroxydiazinon. The six of them are the same as those in our study, which are: diazoxon, triethyl phosphate, triethyl thiophosphate, 2-isopropyl-5-ethyl-6-methylpyrimidine-4-ol, 2-isopropyl-6-methylpyrimidine-4-ol (IMP) and hydroxydiazinon.

In another study, Wang and Shih (2015) degraded DZN using a sono-Fenton process and found four by-products: diazoxon, triethyl phosphate, 2-isopropyl-6-methylpyrimidine-4-ol, and hydroxydiazinon, compounds also found in this work. Wang and Shih (2015) and Molla et al. (2019) performed their experiments with initial DZN concentrations of 50 and 10 $mg.L^{-1}$, respectively, much greater than the concentration used in the present study (1 $mg.L^{-1}$). This lower concentration represents a more logical approximation of realistic wastewater concentrations. Furthermore, while we observed complete mineralization within 30 min, Molla et al. (2019) observed complete mineralization in 20 hours while Wang and Shih (2015) achieved only 30% of mineralization.

In the present study, the GC-MS/MS analysis method combined with the QuEChERS extraction approach and the pre-concentration method showed excellent performance in detecting by-products even at concentrations on the order of $ng.L^{-1}$. This methodology could be used to detect pesticides (at trace levels) and their by-products in waters at ultra-trace levels. Furthermore, as already mentioned, our concentrations of DZN, and associated by products during our degradation process approximate more closely realistic concentrations than the earlier investigations.

Table 2

3.5. Pathways for degradation of diazinon

Several previous studies have suggested a DZN degradation pathway (Molla et al., 2019; Wang and Shih, 2015; Lee et al., 2020). The degradation mechanism of DZN is quite a complex process. Indeed, the number of intermediates and their nature let think that the degradation may be carried out according to several mechanisms, involving several oxidizing species. Hydroxylation, oxidation and hydrolysis are the more probable mechanisms of the DZN degradation. In the Figure 4, an overall scheme includes different routes of by-products formation and their disappearance on basis of the present work and previous reports. Due to the action of the hydroxyl radicals the degradation of DZN involved mainly hydroxylation (Wang and Wang, 2020). In this first step, the hydroxylation of DZN produces hydroxydiazinon, which degrades into other by-products along three different paths.

In the path A, the degradation of hydroxydiazinon involves the cleavage of the C-O bond, producing 2-isopropyl-6-methyl-pyrimidine-4-ol (IMP), which is the most detected by-product in the present study. This compound later degrades to 2-isopropyl-5-ethyl-6-methylprymidine-4-ol. The second route (B) proceeds in parallel with the first (A), and the hydroxydiazinon degrades into triethyl thiophosphate (TTP). It must be noted that the formation of IMP and TTP may occur by hydrolysis mechanism. After this step, TTP releases the sulfate ion and produces triethyl phosphate (TP). The last path proposed (C) is a degradation based on the C–O bond's cleavage combined with conversion of the thiophosphate ester into phosphate ester, whereby the hydroxydiazinon degrades by forming diazoxon. This is due probably to an oxidative mechanism providing diazoxon which undergoes hydrolyze to provide TP and IMP (Lee et al., 2020). Triethyl phosphate is then produced via IMP or another route, which also degrades into 2-isopropyl-5-ethyl-6-methylprymidine-4-ol (Fig. 4).

Figure 4

In Table 3 the effectiveness of degradation/elimination of DZN are compared from several studies including our work. All the cited references were performed at initial DZN concentrations between 10 to 50 $mg.L^{-1}$. The present work targeted depollution of water

containing very low amounts of DZN, on the order of 1 $\mu g.mL^{-1}$. Table 3 provides several techniques used to treat water polluted by DZN. Hassan et al. (2017) used a coupling process of adsorption and photocatalysis, and after 80 min of contact time, the yield of elimination achieved was 95%. Maleki et al. (2020) synthesized a new catalyst for photocatalysis that degraded 99% of DZN in 180 min. The biological treatment employed by Nasrollahi et al. (2020) degraded 55% of DZN but, like other previous studies, requiring greater time. The membrane technique as an elimination process was developed by Pordel et al. (2019), in which they removed 84% of DZN. A few investigations have used advanced oxidation processes. Wang and Shih (2015) coupled the Fenton and sonolysis processes and 98% of DZN degradation was obtained after 60 min with 30% of total mineralization. In contrast, Gar Alalm et al. (2015) utilized photodegradation by applying the photo-Fenton and photocatalysis processes under solar irradiation. They achieved a DZN degradation yield of 50% and 39% after 120 min and 150 min for photo-Fenton and photocatalysis, respectively. Invariably, these works focused on DZN at a relatively high initial concentration, the elimination of which generally exceeded 60 min (Table 3).

Table 3

In this work, both the Fenton and the photo-Fenton processes showed excellent performance, 80% of DZN was degraded using Fenton process after 30 min, and total degradation and mineralization (diazinon and by-products) were obtained by the photo-Fenton after 5 min and 15 min, respectively. Comparing the previous results obtained in the cases of different processes applied to treat contaminated water by DZN, it is obvious that the kinetics of degradation is faster at low concentration of pollutant; this result was already reported in the literature (Lee et al., 2020). These results also reveal a high efficiency of the Fenton and photo-Fenton as degradation techniques for the aqueous solution containing DZN at low level of concentrations.

4. Conclusion

This study investigated the degradation of DZN in water by two types of advanced oxidation processes: Fenton and photo-Fenton. The application of the Doehlert design as an experimental methodology for the optimization of the experimental parameters of the two processes allowed us to develop two mathematical regression models for each process and then determine the corresponding optimal points. Under these conditions, complete degradation of diazinon and by-products was obtained after only 5 min using the photo-

Fenton process. Utilization of the Fenton process allowed for 85% degradation yield after 60 min. All experiments included an initial DZN concentration of 1 $mg.L^{-1}$, a realistic wastewater concentration. By-product identification was carried out using a new method based on the QuEChERS extraction, pre-concentration, and GC-MS/MS analysis. This methodology allowed us to determine the photodegradation by-products even at very low concentrations ($ng.L^{-1}$). DZN degradation using the photo-Fenton process generated six different by-products and 3 degradation paths have been proposed.

Acknowledgement

The authors acknowledge the General Directorate for Scientific Research and Technological Development (DGRSDT), Algeria, for facilitating the funding of the current research work and for providing the necessary support for the completion of this work. This work was carried out as part of the PNE research program. The GC-MS/MS and the UHPLC/DAD were co-founded by the Interreg DOC2C'S project, the CPER Climibio, the region "Hauts-de-France", the French Ministry of Higher Education and the Research and the European Regional Development.

Credit author's statement

Chemseddine Zekkaoui: Data curation, Formal analysis, Methodology, Software, Writing-original draft; **Tarek Berrama**: Supervision, Conceptualization, Formal analysis, Methodology, Software, Validation, Writing-original draft, Writing-review & editing; **David Dumoulin**: Writing-review & editing; **Gabriel Billon**: Writing – review & editing; **Yassine Kadmi**: Supervision, Data curation, Conceptualization, Formal analysis, Methodology, Software, Validation, Writing-review & editing.

Declaration of competing interest

The authors declare that they have no known competing financial interests or personal relationships that could have appeared to influence the work reported in this paper.

References

Abdel Ghani, S., Hanafi, A., 2016. QuEChERS method combined with GC–MS for pesticide residues determination in water. J. Anal. Chem. 71, 508–512. https://doi.org/10.1134/S1061934816050117

Acero, J.L., Benítez, F.J., Real, F.J., González, M., 2008. Chlorination of organophosphorus pesticides in natural waters. J. Hazard. Mater. 153, 320–328. https://doi.org/10.1016/j.jhazmat.2007.08.051

Al Momani, F., Gonzalez, O., Sans, C., Esplugas, S., 2004a. Combining photo-Fenton process with biological sequencing batch reactor for 2,4-dichlorophenol degradation. Water Sci. Technol. 49, 293–298. https://doi.org/10.2166/wst.2004.0288

Al Momani, F., Sans, C., Esplugas, S., 2004b. A comparative study of the advanced oxidation of 2,4-dichlorophenol. J. Hazard. Mater. 107, 123–129. https://doi.org/10.1016/j.jhazmat.2003.11.015

Al Momani, F.A., Shawaqfeh, A.T., Al-Zoubi, H., 2009. Comparison of different treatment alternatives for removal of pesticide from water solution. J. Chem. Technol. Biotechnol. 85, 529-535. https://doi.org/10.1002/jctb.2324

Al Momani, F.A., Shawaqfeh, A.T., Shawaqfeh, M.S., 2007. Solar wastewater treatment plant for aqueous solution of pesticide. Sol. Energy. 81, 1213–1218. https://doi.org/10.1016/j.solener.2007.01.007

Ameta, R., K. Chohadia, A., Jain, A., Punjabi, P.B., 2018. Fenton and Photo-Fenton Processes, in: Advanced Oxidation Processes for Waste Water Treatment, 49–87. https://doi.org/10.1016/B978-0-12-810499-6.00003-6

Audino, F., Conte, L., Schenone, A., Pérez-Moya, M., Graells, M., Alfano, O.M., 2017. A Kinetic Study for the Fenton and Photo-Fenton Paracetamol Degradation in a Pilot Plant Reactor, in: Computer Aided Chemical Engineering, 301–306. https://doi.org/10.1016/B978-0-444-63965-3.50052-0

Benredouane, S., Berrama, T., Doufene, N., 2016. Strategy of screening and optimization of process parameters using experimental design: application to amoxicillin elimination by adsorption on activated carbon. Chemom. Intell. Lab. Syst. 155, 128–137.

Callao, M.P., 2014. Multivariate experimental design in environmental analysis. TrAC Trends Anal. Chem. 62, 86–92. https://doi.org/10.1016/j.trac.2014.07.009

Čolović, M., Krstić, D., Petrović, S., Leskovac, A., Joksić, G., Savić, J., Franko, M., Trebše, P., Vasić, V., 2010. Toxic effects of diazinon and its photodegradation products. Toxicol. Lett. 193, 9–18. https://doi.org/10.1016/j.toxlet.2009.11.022

Daneshvar, N., Aber, S., Seyeddorraji, M., Khataee, A., Rasoulifard, M., 2007. Photocatalytic degradation of the insecticide diazinon in the presence of prepared nanocrystalline ZnO powders under irradiation of UV-C light. Sep. Purif. Technol. 58, 91–98. https://doi.org/10.1016/j.seppur.2007.07.016

de Souza, R.M., Seibert, D., Quesada, H.B., de Jesus Bassetti, F., Fagundes-Klen, M.R., Bergamasco, R., 2020. Occurrence, impacts and general aspects of pesticides in surface water: A review. Process Saf. Environ. Prot. 135, 22–37. https://doi.org/10.1016/j.psep.2019.12.035

505 Doufene, N., Berrama, T., Tahtat, D., Benredouane, S., Nekaa, C., 2018. Combination of Two
506 Experimental Designs to Optimize the Dimethylphthalate Elimination on Activated Carbon
507 Elaborated from Arundo donax. Arab. J. Sci. Eng. https://doi.org/10.1007/s13369-018-3531-5

508 Dragoi, E.N., Vasseghian, Y., 2020. Modeling of mass transfer in vacuum membrane
509 distillation process for radioactive wastewater treatment using artificial neural networks.
510 Toxin Rev. 0, 1–10. https://doi.org/10.1080/15569543.2020.1744659

511 Drożdżyński, D., Kowalska, J., 2009. Rapid analysis of organic farming insecticides in soil
512 and produce using ultra-performance liquid chromatography/tandem mass spectrometry.
513 Anal. Bioanal. Chem. 394, 2241–2247. https://doi.org/10.1007/s00216-009-2931-5

514 Fernanda Pereira Barbosa, P., 2019. Voltammetric Techniques for Pesticides and Herbicides
515 Detection- an Overview. Int. J. Electrochem. Sci. 3418–3433.
516 https://doi.org/10.20964/2019.04.60

517 Ferreira, S., 2004. Doehlert matrix: a chemometric tool for analytical chemistry?review.
518 Talanta 63, 1061–1067. https://doi.org/10.1016/j.talanta.2004.01.015

519 Ferreira, S.L.C., Bruns, R.E., da Silva, E.G.P., dos Santos, W.N.L., Quintella, C.M., David,
520 J.M., de Andrade, J.B., Breitkreitz, M.C., Jardim, I.C.S.F., Neto, B.B., 2007. Statistical
521 designs and response surface techniques for the optimization of chromatographic systems. J.
522 Chromatogr. A 1158, 2–14. https://doi.org/10.1016/j.chroma.2007.03.051

523 Gar Alalm, M., Tawfik, A., Ookawara, S., 2015. Comparison of solar TiO 2 photocatalysis
524 and solar photo-Fenton for treatment of pesticides industry wastewater: Operational
525 conditions, kinetics, and costs. J. Water Process Eng. 8, 55–63.
526 https://doi.org/10.1016/j.jwpe.2015.09.007

527 Glinski, D.A., Purucker, S.T., Van Meter, R.J., Black, M.C., Henderson, W.M., 2018.
528 Analysis of pesticides in surface water, stemflow, and throughfall in an agricultural area in
529 South Georgia, USA. Chemosphere 209, 496–507.
530 https://doi.org/10.1016/j.chemosphere.2018.06.116

531 Hanrahan, G., Lu, K., 2006. Application of Factorial and Response Surface Methodology in
532 Modern Experimental Design and Optimization. Crit. Rev. Anal. Chem. 36, 141–151.
533 https://doi.org/10.1080/10408340600969478

534 Hassan, A.F., Elhadidy, H., Abdel-Mohsen, A.M., 2017. Adsorption and photocatalytic
535 detoxification of diazinon using iron and nanotitania modified activated carbons. J. Taiwan
536 Inst. Chem. Eng. 75, 299–306. https://doi.org/10.1016/j.jtice.2017.03.026

537 Heydari, M., Karimyan, K., Darvish Motevalli, M., Karami, A., Vasseghian, Y., Azizi, N.,
538 Ghayebzadeh, M., Moradi, M., 2018. Data for efficiency comparison of raw pumice and
539 Manganese-modified pumice for removal phenol from aqueous environments-Application of
540 response surface methodology. Data Brief 20. https://doi.org/10.1016/j.dib.2018.09.027

Iqbal, S., Iqbal, M.M., Javed, M., Bahadur, A., Yasien, S., Najam-ud-din, Hurr, A., Ahmad, N., Raheel, M., Liu, G., 2020. Modified QuEChERS extraction method followed by simultaneous quantitation of nine multi-class pesticides in human blood and urine by using GC-MS. J. Chromatogr. B 1152, 122227. https://doi.org/10.1016/j.jchromb.2020.122227

Jones, L., Kinsella, B., Forde, K., Furey, A., Regan, F., 2017. A robust analytical method for the determination of pesticide residues in wastewater. Anal. Methods 9, 4167–4174. https://doi.org/10.1039/C7AY00704C

Kanakaraju, D., Glass, B.D., Oelgemöller, M., 2018. Advanced oxidation process-mediated removal of pharmaceuticals from water: A review. J. Environ. Manage. 219, 189–207. https://doi.org/10.1016/j.jenvman.2018.04.103

Katsikantami, I., Colosio, C., Alegakis, A., Tzatzarakis, M.N., Vakonaki, E., Rizos, A.K., Sarigiannis, D.A., Tsatsakis, A.M., 2019. Estimation of daily intake and risk assessment of organophosphorus pesticides based on biomonitoring data – The internal exposure approach. Food Chem. Toxicol. 123, 57–71. https://doi.org/10.1016/j.fct.2018.10.047

Kaur, R., Mavi, G.K., Raghav, S., Khan, I., 2019. Pesticides Classification and its Impact on Environment. Int. J. Curr. Microbiol. Appl. Sci. 8, 1889–1897. https://doi.org/10.20546/ijcmas.2019.803.224

Kazemizad, L., Ghaffari, Y., Kermani, M., Farzadkia, M., Hajizadeh, A., 2016. Investigation of Photo–Fenton–Like Process Efficiency in Diazinon Pesticide Removal from Aqueous Solutions. J. Saf. Environ. Health Res. 1. https://doi.org/10.22053/jsehr.2016.33383

Lee, Y., Kim, Y., Khan, M.S.I., Na, Y.C., 2020. Identification and determination of by-products originating from ozonation of chlorpyrifos and diazinon in water by liquid chromatography–mass spectrometry. J. Sep. Sci. 43, 4047–4057. https://doi.org/10.1002/jssc.202000584

Malakootian, M., Shahesmaeili, A., Faraji, M., Amiri, H., Silva Martinez, S., 2020. Advanced oxidation processes for the removal of organophosphorus pesticides in aqueous matrices: A systematic review and meta-analysis. Process Saf. Environ. Prot. 134, 292–307. https://doi.org/10.1016/j.psep.2019.12.004

Maleki, A., Moradi, F., Shahmoradi, B., Rezaee, R., Lee, S.-M., 2020. The photocatalytic removal of diazinon from aqueous solutions using tungsten oxide doped zinc oxide nanoparticles immobilized on glass substrate. J. Mol. Liq. 297, 111918. https://doi.org/10.1016/j.molliq.2019.111918

Marchetti, M.D., Bessa Azevedo, E., 2020. Degradation of NSAIDs by optimized photo-Fenton process using UV-LEDs at near-neutral pH. J. Water Process Eng. 35, 101171. https://doi.org/10.1016/j.jwpe.2020.101171

576 Metcalfe, C.D., Helm, P., Paterson, G., Kaltenecker, G., Murray, C., Nowierski, M., Sultana,
577 T., 2019. Pesticides related to land use in watersheds of the Great Lakes basin. Sci. Total
578 Environ. 648, 681–692. https://doi.org/10.1016/j.scitotenv.2018.08.169

579 Mirzaei, A., Chen, Z., Haghighat, F., Yerushalmi, L., 2017. Removal of pharmaceuticals from
580 water by homo/heterogonous Fenton-type processes – A review. Chemosphere 174, 665–688.
581 https://doi.org/10.1016/j.chemosphere.2017.02.019

582 Molla, Md.A.I., Furukawa, M., Tateishi, I., Katsumata, H., Kaneco, S., 2019. Mineralization
583 of Diazinon with nanosized-photocatalyst TiO_2 in water under sunlight irradiation:
584 optimization of degradation conditions and reaction pathway. Environ. Technol. 1–10.
585 https://doi.org/10.1080/09593330.2019.1615129

586 Moradi, M., Elahinia, A., Vasseghian, Y., Dragoi, E. N., Omidi, F., Mousavi Khaneghah, A.,
587 2020a. A review on pollutants removal by Sono-photo -Fenton processes. J. Environ. Chem.
588 Eng. 8, 104330. https://doi.org/10.1016/j.jece.2020.104330

589 Moradi, M., Heydari, M., Darvishmotevalli, M., Karimyan, K., Gupta, V.K., Vasseghian, Y.,
590 Sharafi, H., 2018. Kinetic and modeling data on phenol removal by Iron-modified Scoria
591 Powder (FSP) from aqueous solutions. Data Brief 20, 957–968.
592 https://doi.org/10.1016/j.dib.2018.08.068

593 Moradi, M., Vasseghian, Y., Arabzade, H., Mousavi Khaneghah, A., 2021. Various
594 wastewaters treatment by sono-electrocoagulation process: A comprehensive review of
595 operational parameters and future outlook. Chemosphere 263, 128314.
596 https://doi.org/10.1016/j.chemosphere.2020.128314

597 Moradi, M., Vasseghian, Y., Khataee, A., Kobya, M., Arabzade, H., Dragoi, E.N., 2020b.
598 Service life and stability of electrodes applied in electrochemical advanced oxidation
599 processes: A comprehensive review. J. Ind. Eng. Chem. 87, 18–39.
600 https://doi.org/10.1016/j.jiec.2020.03.038

601 Nasrollahi, M., Pourbabaei, A.A., Etesami, H., Talebi, K., 2020. Diazinon degradation by
602 bacterial endophytes in rice plant (Oryzia sativa L.): A possible reason for reducing the
603 efficiency of diazinon in the control of the rice stem–borer. Chemosphere 246, 125759.
604 https://doi.org/10.1016/j.chemosphere.2019.125759

605 Nichela, D.A., Berkovic, A.M., Costante, M.R., Juliarena, M.P., García Einschlag, F.S., 2013.
606 Nitrobenzene degradation in Fenton-like systems using Cu(II) as catalyst. Comparison
607 between Cu(II)- and Fe(III)-based systems. Chem. Eng. J. 228, 1148–1157.
608 https://doi.org/10.1016/j.cej.2013.05.002

609 Organización Mundial de la Salud, 2010. The WHO recommended classification of pesticides
610 by hazard and guidelines to classification 2009. WHO, Geneva.

611 Pordel, M.A., Maleki, A., Ghanbari, R., Rezaee, R., Khamforoush, M., Daraei, H., Athar,
612 S.D., Shahmoradi, B., Safari, M., Ziaee, A. hossein, Lalhmunsiama, Lee, S.-M., 2019.

Evaluation of the effect of electrospun nanofibrous membrane on removal of diazinon from aqueous solutions. React. Funct. Polym. 139, 85–91. https://doi.org/10.1016/j.reactfunctpolym.2019.03.017

Proia, L., Osorio, V., Soley, S., Köck-Schulmeyer, M., Pérez, S., Barceló, D., Romaní, A.M., Sabater, S., 2013. Effects of pesticides and pharmaceuticals on biofilms in a highly impacted river. Environ. Pollut. 178, 220–228. https://doi.org/10.1016/j.envpol.2013.02.022

Raeisi, A., Arfaeinia, H., Seifi, M., Shirzad-Siboni, M., Keshtkar, M., Dobaradaran, S., 2016. Polycyclic aromatic hydrocarbons (PAHs) in coastal sediments from urban and industrial areas of Asaluyeh Harbor, Iran: distribution, potential source and ecological risk assessment. Water Sci. Technol. 74, 957–973. https://doi.org/10.2166/wst.2016.265

Rahim Pouran, S., Abdul Aziz, A.R., Wan Daud, W.M.A., 2015. Review on the main advances in photo-Fenton oxidation system for recalcitrant wastewaters. J. Ind. Eng. Chem. 21, 53–69. https://doi.org/10.1016/j.jiec.2014.05.005

Real, F.J., Benitez, F.J., Acero, J.L., Gonzalez, M., 2007. Removal of diazinon by various advanced oxidation processes. J. Chem. Technol. Biotechnol. 82, 566–574. https://doi.org/10.1002/jctb.1702

Sadowski, A., Baer-Nawrocka, A., 2018. Food and environmental function in world agriculture—Interdependence or competition? Land Use Policy 71, 578–583. https://doi.org/10.1016/j.landusepol.2017.11.005

Shirzad-Siboni, M., Khataee, A., Vahid, B., Joo, S.W., 2015. Synthesis, Characterization and Immobilization of ZnO Nanosheets on Scallop Shell for Photocatalytic Degradation of an Insecticide. Sci. Adv. Mater. 7, 806–814. https://doi.org/10.1166/sam.2015.2163

Singh, J., Sharma, S., Aanchal, Basu, S., 2019. Synthesis of Fe2O3/TiO2 monoliths for the enhanced degradation of industrial dye and pesticide via photo-Fenton catalysis. J. Photochem. Photobiol. Chem. 376, 32–42. https://doi.org/10.1016/j.jphotochem.2019.03.004

Smaali, A., Berkani, M., Merouane, F., Le, V.T., Vasseghian, Y., Rahim, N., Kouachi, M., 2021. Photocatalytic-persulfate- oxidation for diclofenac removal from aqueous solutions: Modeling, optimization and biotoxicity test assessment. Chemosphere 266, 129158. https://doi.org/10.1016/j.chemosphere.2020.129158

Vasseghian, Y., Moradi, M., Pirsaheb, M., Khataee, A., Rahimi, S., Badi, M.Y., Mousavi Khaneghah, A., 2020. Pesticide decontamination using UV/ferrous-activated persulfate with the aid neuro-fuzzy modeling: A case study of Malathion. Food Res. Int. 137, 109557. https://doi.org/10.1016/j.foodres.2020.109557

Vasseghian, Y., Khataee, A., Dragoi, E.N., Moradi, M., Nabavifard, S., Oliveri Conti, G., Mousavi Khaneghah, 2020. Pollutants degradation and power generation by photocatalytic fuel cells: A comprehensive review. Arab. J. Chem. 13, 8458–8480. https://doi.org/10.1016/j.arabjc.2020.07.016

650 Vasseghian, Y., Berkani, M., Almomani, F., Dragoi, E. N., 2021. Data mining for pesticide
651 decontamination using heterogeneous photocatalytic processes. Chemosphere 270, 129449.
652 https://doi.org/10.1016/j.chemosphere.2020.129449

653 Wang, C., Shih, Y., 2015. Degradation and detoxification of diazinon by sono-Fenton and
654 sono-Fenton-like processes. Sep. Purif. Technol. 140, 6–12.
655 https://doi.org/10.1016/j.seppur.2014.11.005

656 Wang, J., Wang, S., 2020. Reactive species in advanced oxidation processes: Formation,
657 identification and reaction mechanism. Chem. Eng. J. 401, 126158.
658 https://doi.org/10.1016/j.cej.2020.126158

659 Zaidon, S.Z., Ho, Y.B., Hamsan, H., Hashim, Z., Saari, N., Praveena, S.M., 2019. Improved
660 QuEChERS and solid phase extraction for multi-residue analysis of pesticides in paddy soil
661 and water using ultra-high performance liquid chromatography tandem mass spectrometry.
662 Microchem. J. 145, 614–621. https://doi.org/10.1016/j.microc.2018.11.025

663 Zhang, Y., Zhang, W., Liao, X., Zhang, J., Hou, Y., Xiao, Z., Chen, F., Hu, X., 2010.
664 Degradation of diazinon in apple juice by ultrasonic treatment. Ultrason. Sonochem. 17, 662–
665 668. https://doi.org/10.1016/j.ultsonch.2009.11.007

666

List of figures

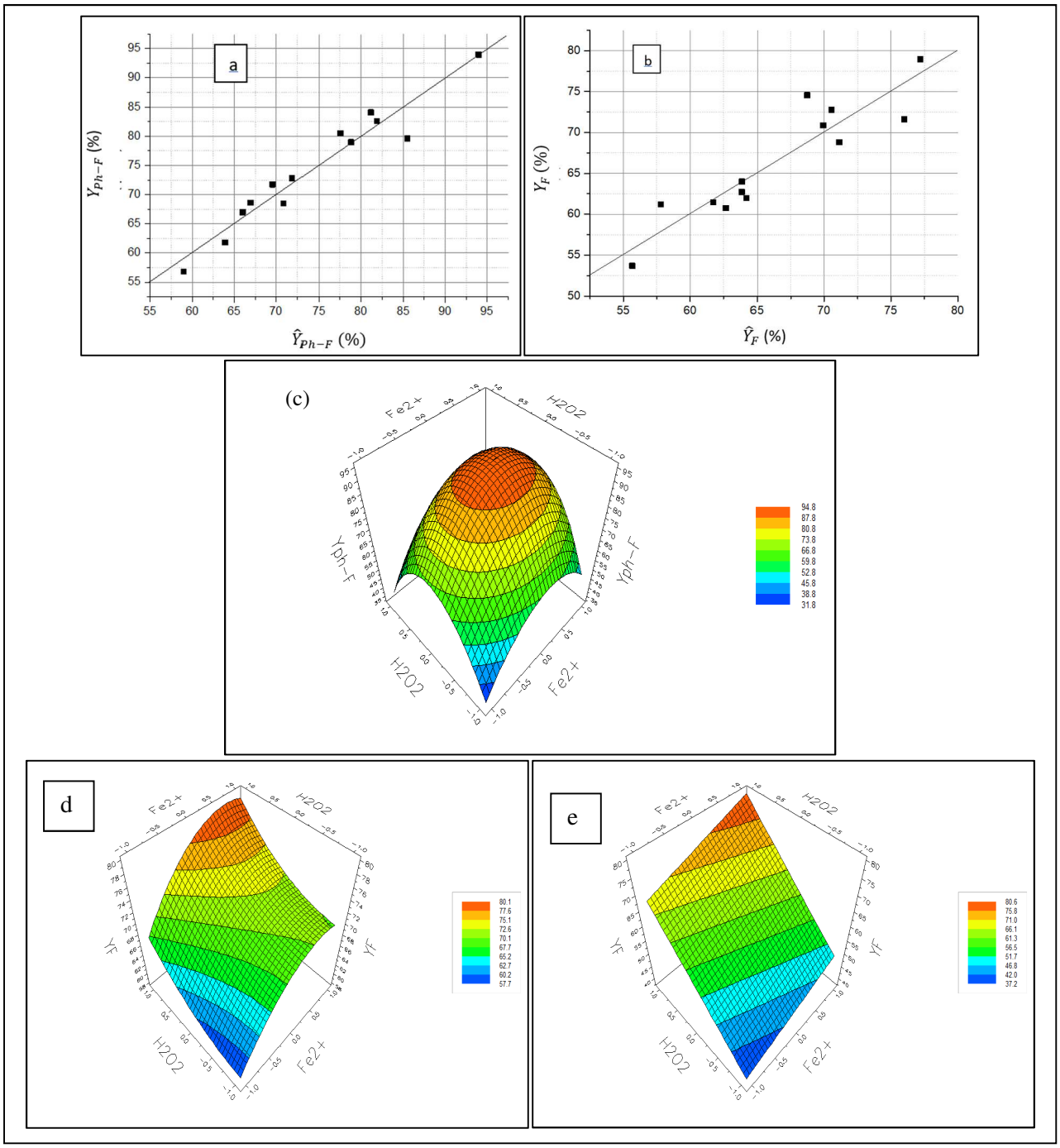

Figure 1. Experimental versus predicted values for (a) Photo-Fenton process, (b) Fenton process, and 3D response surface plots for (c) Photo-Fenton process, (d) and (e) Fenton process.

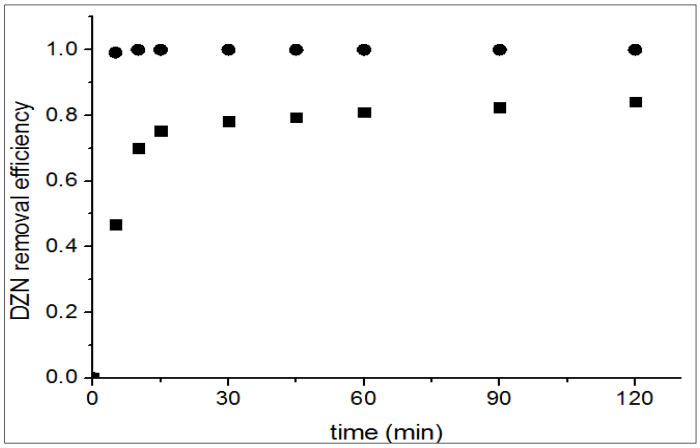

Figure 2. Kinetics of diazinon degradation under optimal conditions for: ■ Fenton and ● Photo-Fenton.

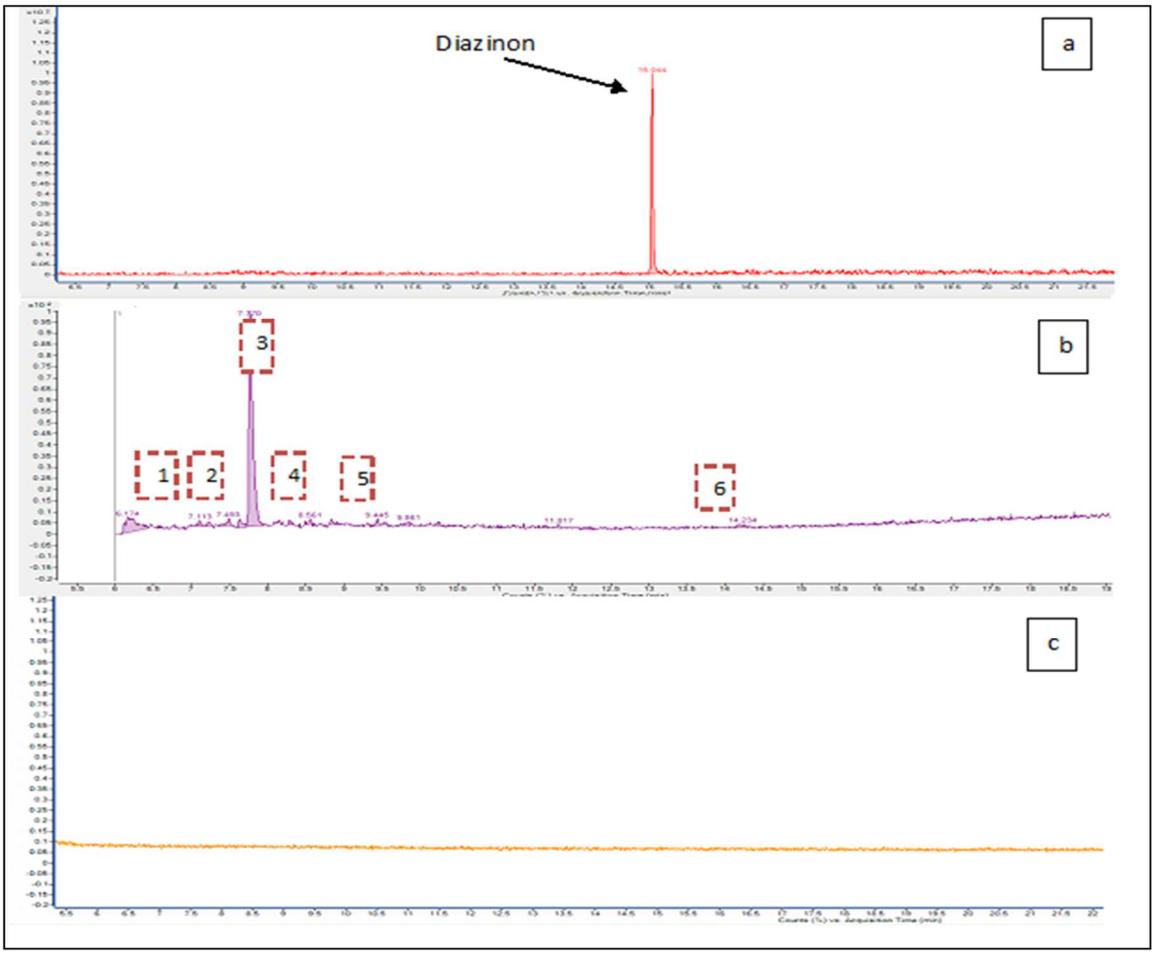

Figure 3. Chromatograms obtained by GC-MS/MS, (a). before Photo-Fenton degradation, (b). after 5 min of Photo-Fenton process and (c) after 60 min of Photo-Fenton degradation.

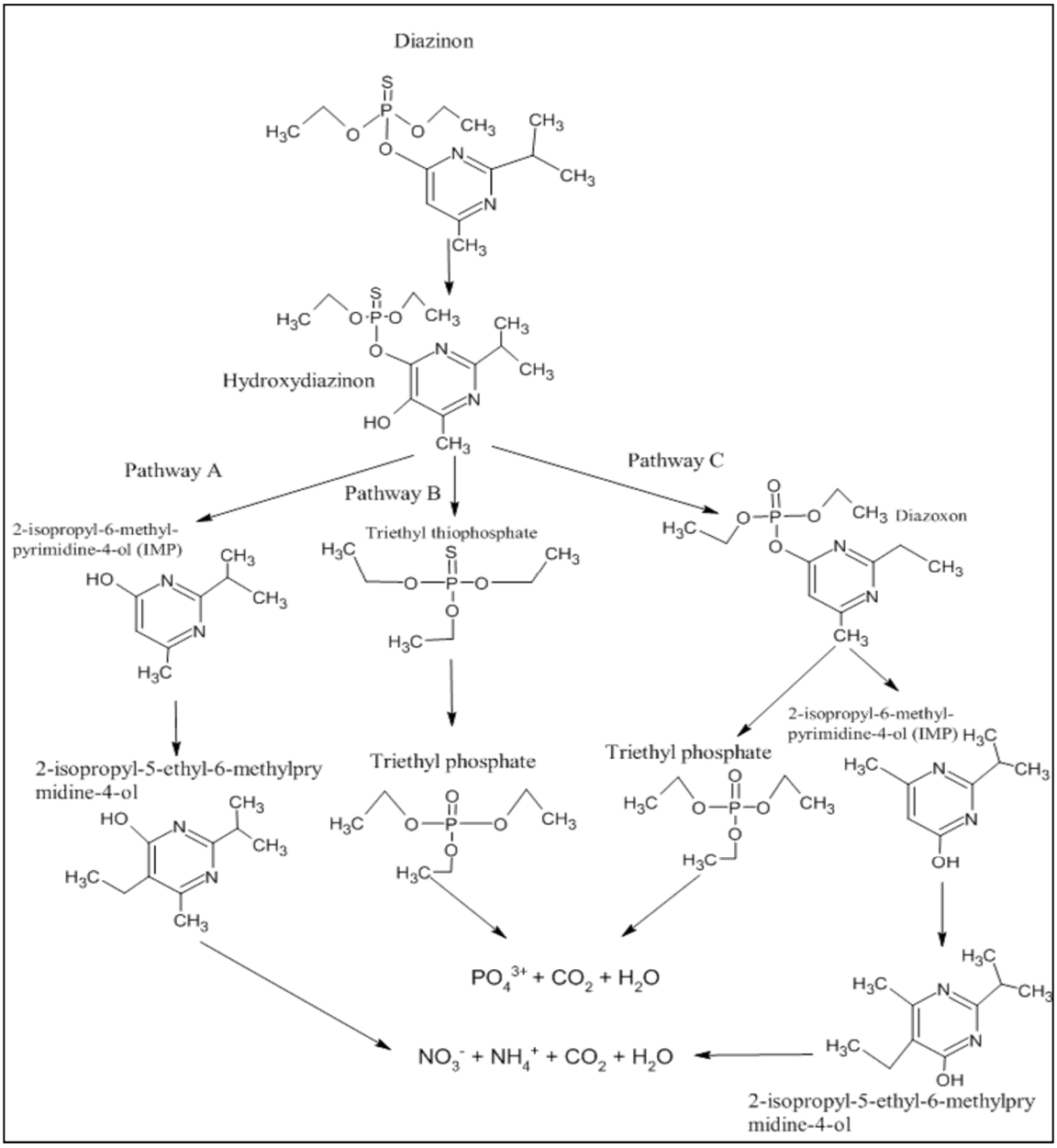

Figure 4. Proposed degradation pathways of DZN.

List of tables

Table 1. Experimental matrix of Doehlert and the corresponding measured responses.

Run	Coded value X_1	Actual value $[Fe^{2+}]$ (mg. L^{-1})	Coded value X_2	Actual value $[H_2O_2]$ (mg. L^{-1})	Coded value X_3	Actual value pH	Yield (%)	
							Photo-Fenton	Fenton
1	0.000	25.0	0.000	250.0	0.000	5.00	93.98	70.86
2	+1.000	45.0	0.000	250.0	0.000	5.00	82.59	71.60
3	+0.500	35.0	+0.866	423.2	0.000	5.00	72.79	78.96
4	-0.500	15.0	+0.866	423.2	0.000	5.00	61.81	68.81
5	-1.000	5.0	0.000	250.0	0.000	5.00	67.00	64.00
6	-0.500	15.0	-0.866	76.8	0.000	5.00	56.83	60.74
7	+0.500	35.0	-0.866	76.8	0.000	5.00	68.61	74.56
8	+0.500	35.0	+0.289	307.8	+0.816	6.63	78.98	62.72
9	-0.500	15.0	+0.289	307.8	+0.816	6.63	68.50	61.19
10	0.000	25.0	-0.577	134.6	+0.816	6.63	71.75	61.99
11	+0.500	35.0	-0.289	192.2	-0.816	3.37	79.64	61.47
12	-0.500	15.0	-0.289	192.2	-0.816	3.37	80.51	53.69
13	0.000	25.0	+0.577	365.4	-0.816	3.37	84.06	72.77

Table 2. Comparison studies of works aimed at the degradation and/or elimination of diazinon.

Process	Conditions	Method of analysis	Elimination/ degradation yield (%)	References
Adsorption/ Photocatalysis	C_0 = 40 mg.L^{-1} TiO_2-AC = 1 g.L^{-1} t = 80 min TiO_2 = 1 g.L^{-1} t = 80 min	UV/Vis spectrophotometer Unicam UV/Vis 5625, at a wavelength of 247 nm	95 55	(Hassan et al., 2017)
Photocatalysis	C_0 = 10 mg.L^{-1} WO_3 doped ZnO 10 mg/cm^{-2} 2% t = 180 min Neutral pH	Gas Chromatography/ Flame Ionization Detector (GC/FID)	99	(Maleki et al., 2020)
Sono-Fenton	C_0 = 50 mg.L^{-1} f = 20 khz C_{Fe} = 20 mg.L^{-1} $C_{H_2O_2}$ = 150 mg.L^{-1} pH = 3 t = 60 min	Gas Chromatography/ Flame Ionization Detector (GC/FID)	98.3 (degradation) 29.9 (mineralization)	(Wang and Shih, 2015)
Solar photo-Fenton	Real industrial wastewater C_0 = 11 mg.L^{-1} $C_{H_2O_2}$ = 1 g.L^{-1} C_{Fe} = 3 g.L^{-1} t = 180 min	Shimadzu HPLC using C-18 phenomenex reverse phase column and Diode Array Detector (HPLC/DAD)	50.1	(Gar Alalm et al., 2015)
Photocatalysis	Real industrial wastewater C_0 = 11 mg.L^{-1} TiO_2 = 2 g.L^{-1} pH = 3.8 t = 120 min		38.2	
Biological	C_0 = 20 mg.L^{-1} bacterial endophytes in rice plant	High-Performance Liquid Chromatography-Diode Array Detector (HPLC/DAD)	58.5	(Nasrollahi et al., 2020)
Membrane technique	Electrospun nanofibrous membrane C_0 = 10 mg.L^{-1} pH = 7 0.1% nanoparticules t = 60 min	Spectrophotometer DR 5000 device at 247 nm	83.7	(Pordel et al., 2019)
Fenton	C_0 = 1 µg.mL^{-1} $C_{H_2O_2}$ = 423.2 mg.L^{-1} C_{Fe} = 45 mg.L^{-1} pH = 5 t = 30 min	Ultra High-Performance Liquid Chromatography equipped with a Diode Array Detector (UHPLC/DAD) and gas chromatography coupled with triple quadrupole mass spectrometry (GC-MS/MS)	85	**This work**
Photo-Fenton	C_0 = 1 µg.mL^{-1} $C_{H_2O_2}$ = 262 mg.L^{-1} C_{Fe} = 29 mg.L^{-1} pH = 4.6 t = 5 min		100 Total mineralization	**This work**

Table 3. Identification of DZN degradation by-products with GC-MS/MS.

No.	By-products	Retention time (min)	Molecular weight (m/z)	Compounds
1	Triethyl thiophosphate	7.11	198	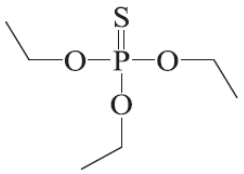
2	2-isopropyl-5-ethyl-6-methylprymidine-4-ol	7.49	156	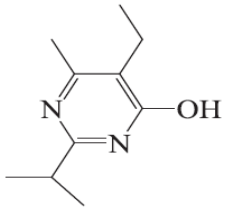
3	2-isopropyl-6-methyl-pyrimidine-4-ol (IMP)	7.77	133	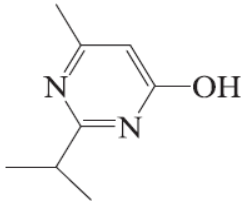
4	Triethyl phosphate	8.56	182	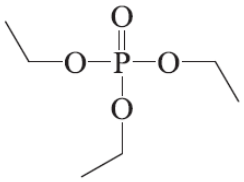
5	Diazoxon	9.44	137	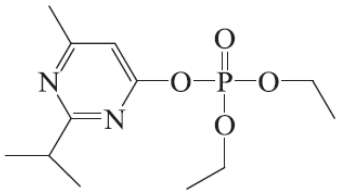
6	Hydroxydiazinon	14.23	178	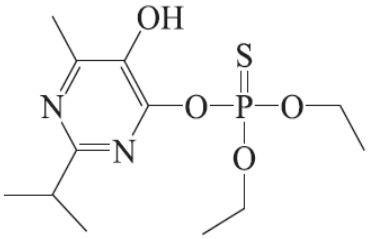

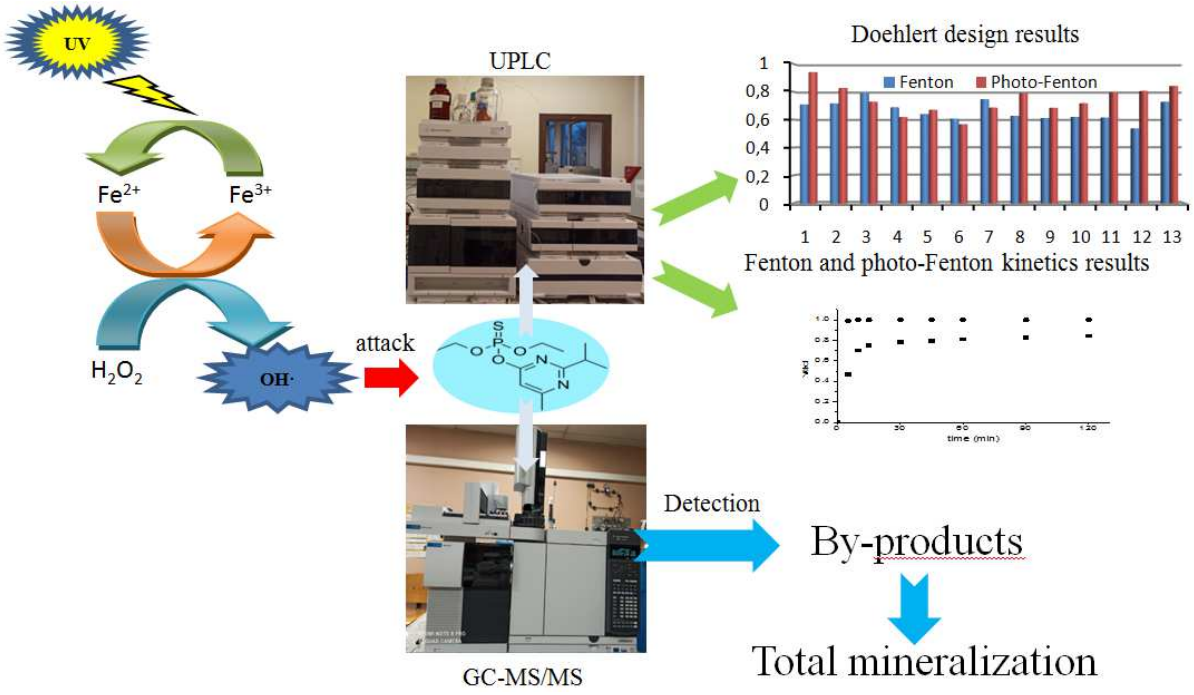
UV
Fe2+
Fe3+
H2O2
OH·
attack
UPLC
GC-MS/MS
Detection
By-products
Total mineralization
Doehlert design results
Fenton
Photo-Fenton
1
0,8
0,6
0,4
0,2
0
1 2 3 4 5 6 7 8 9 10 11 12 13
Fenton and photo-Fenton kinetics results
time (min)